A Letters Journal Exploring the Frontiers of Physics

November 2015

EPL, **112** (2015) 38002 www.epljournal.org
doi: 10.1209/0295-5075/112/38002

Mechanism of quasi-periodic lag jitter in bursting rhythms by a neuronal network

R. Barrio[1,2(a)], Marcos Rodríguez[2,3], S. Serrano[1,2] and Andrey Shilnikov[4,5]

[1] *Departamento de Matemática Aplicada and IUMA, University of Zaragoza - E-50009 Zaragoza, Spain*
[2] *CODY and GME, University of Zaragoza - E-50009 Zaragoza, Spain*
[3] *Centro Universitario de la Defensa - E-50090 Zaragoza, Spain*
[4] *Neuroscience Institute and Department of Mathematics and Statistics, Georgia State University Atlanta, GA, USA*
[5] *Institute for Information Technologies, Mathematics and Mechanics, Lobachevsky State University of Nizhni Novgorod - Nizhni Novgorod, Russia*

received 15 September 2015; accepted in final form 30 October 2015
published online 17 November 2015

PACS 87.19.lj – Neuronal network dynamics
PACS 87.19.ll – Models of single neurons and networks
PACS 87.19.lm – Synchronization in the nervous system

Abstract – We study a heteroclinic bifurcation leading to the onset of robust phase-lag jittering in bursting rhythms generated by a neuronal circuit. We show that the jitter phenomenon is associated with the occurrence of a stable invariant curve emerging through a torus bifurcation in 2D return maps for phase lags between three constituent bursters. To study biologically plausible and phenomenological models of rhythmic neuronal networks we have further developed parallel computational techniques for parameter continuations of all possible fixed points and invariant curves of such return maps. The method is based on a "fine" brute-force analysis of the large data set generated by the computational techniques.

Introduction. – Studies of dynamical complexity exhibited by systems of globally coupled phase oscillators are currently an active research trend [1–3]. In part, this trend has additionally been stimulated by one of the pivotal challenges of the new century —comprehending brain activity. To unravel how such an incredibly sophisticated conglomerate as the brain functions dynamically, it is imperative to fully understand the dynamics of its basic elements —neurons and small neuronal circuits or motifs. Such motifs share the same characteristics detected in oscillator networks [4–6]. In [7] it has been found, later studied in [1,8], that robust "slow switching" oscillations are caused by the presence of heteroclinic attractors emerging through codimension-one heteroclinic bifurcations with symmetry. Oscillatory networks and simple neuronal circuits have been identified to possess such heteroclinic cycles underlying the mechanism of "the winnerless competition principle" [9,10]. These phenomena give rise to robust, sequential repetitions of behaviors in small neuronal networks.

A central pattern generator (CPG) is a neuronal circuit of cells that autonomously produces rhythmic activity underlying repetitive behavioral patterns in animals. CPGs have been identified in many animals, where they have been implicated in the control of diverse behaviors such as heartbeat, sleep, respiration, chewing, and locomotion on land and in water [11–13]. Mathematical studies of reduced CPG models have come up with useful insights shedding light onto some operational principles of biological CPG networks, for example, the swim CPG of a sea mollusk *Melibe leonina* [14,15]. One such insight is a dynamical explanation of phase "jittering" oscillations that are recorded in voltage waveforms with periodically time varying phase lags between burst initiations in the neurons constituting the circuit. It is attributed to the occurrence of a stable invariant curve in the proximity of a heteroclinic cycle composed of several saddles representing phase thresholds. In some cases the explicit equations of the phase shift may be introduced so that with a blend of analytical and continuation techniques one can describe the dynamics of such oscillatory networks [1,3]. However, for most of the plausible CPGs the explicit equations for

(a) E-mail: rbarrio@unizar.es

the phase lags do not exist. Therefore, no computational continuation routine can stably identify heteroclinic cycles in individual and also in coupled systems. There is a class of specific neuronal networks [16–19] in which one can locate equilibria corresponding to phase-locked rhythms and examine stability conditions and their loss using local bifurcation analysis. Because of the limited applicability of this analysis, a new computational technique was proposed in [20–22] that permits one to examine in detail all possible rhythmic states in larger CPG motifs [23].

In this paper we further develop and extend the applicability of the computational suite of aggregated techniques that was initially proposed in [20] to examine nonlocal bifurcations of bursting polyrhythms in small networks of weakly coupled neurons. The suite allows one to computationally perform the parameter continuation to determine all possible rhythms and analyze their bifurcations, local and non-local, occurring in a 3-cell circuit as its intrinsic and coupling parameters are changed. The novelty of the approach is the introduction of implicitly defined Poincaré return maps for phase lags that can be understood geometrically. Later a large number of such Poincaré return maps, obtained for several values of the parameters, generates a large data set that permits to locate all the relevant information, such as bifurcation points. Afterwards, a refinement process is done, where the "exact" parameter value at which the event takes place is automatically obtained. So, this is an example of "fine" brute-force analysis in neuronal circuits. This paper presents the methodology and applies it, as an example, to the precise location of "phase jitter" phenomena and the bifurcations that give rise to its appearance (through a secondary Andronov-Hopf bifurcation followed by the formation of a heteroclinic cycle).

3-cell neuronal network. – We consider an inhibitory neuronal circuit constituted by three endogenous bursters [20,24] of the Hodgkin-Huxley type [25] that describes bursting phenomena in leech heart neurons [24]:

$$\begin{cases} CV' = -I_{\rm Na} - I_{\rm K2} - I_{\rm L} - I_{\rm app} - I_{\rm syn}, \\ \tau_{\rm Na}\ h'_{\rm Na} = h^{\infty}_{\rm Na}(V) - h_{\rm Na}, \\ \tau_{\rm K2} m'_{\rm K2} = m^{\infty}_{\rm K2}(V) - m_{\rm K2}, \end{cases} \tag{1}$$

with $I_{\rm L} = \bar{g}_{\rm L}(V - {\rm E_L})$, $I_{\rm K2} = \bar{g}_{\rm K2}$, $m^2_{\rm K2}(V - {\rm E_{K2}})$, $m_{\rm Na} = m^{\infty}_{\rm Na}(V)$, $I_{\rm Na} = \bar{g}_{\rm Na}\, m^3_{\rm Na} h_{\rm Na}(V - {\rm E_{Na}})$, where C is the membrane capacitance; V is the membrane potential; $I_{\rm Na}$ is the fast voltage gated sodium current with slow inactivation $h_{\rm Na}$ and fast activation $m_{\rm Na}$; $I_{\rm K2}$ is the persistent potassium current with activation $m_{\rm K2}$; $I_{\rm L}$ is the leak current and $I_{\rm app}$ is a constant polarization or external applied current. The term $I_{\rm syn}$ is the coupling factor via fast chemical synapses. In the simulations of the isolated neuron $I_{\rm syn} = 0$. The values of the fixed parameters in the model used in this paper are ${\rm E_{Na}} = 0.045$, $\bar{g}_{\rm Na} = 160$, ${\rm E_{K2}} = -0.07$, $\bar{g}_{\rm K2} = 30$, ${\rm E_L} = -0.046$, $\bar{g}_{\rm L} = 8$, $C = 0.5$, $\tau_{\rm Na} = 0.0405$ and $\tau_{\rm K2} = 0.9$. The steady-state values of

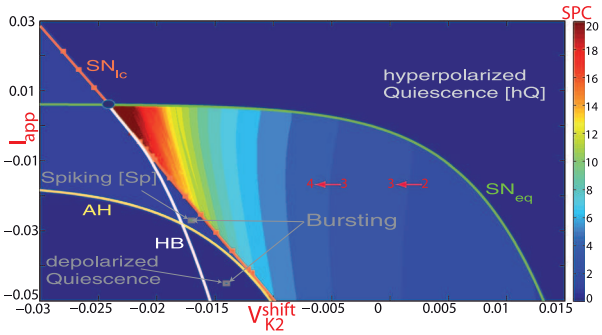

Fig. 1: (Color online) $(V^{\tt shift}_{\rm K2}, I_{\rm app})$-parametric sweep using the spike-counting method (color-coded bar on the right for the spike range) with the superimposed bifurcation lines (for Andronov-Hopf, saddle-node and homoclinic bifurcations) demarcating the regions of bursting, tonic-spiking and quiescent activity in individual neurons.

gating variables are given by the experimentally calibrated Boltzmann functions:

$$\begin{aligned} h^{\infty}_{\rm Na}(V) &= [1 + \exp(500(V + 0.0325))]^{-1}, \\ m^{\infty}_{\rm Na}(V) &= [1 + \exp(-150(V + 0.0305))]^{-1}, \\ m^{\infty}_{\rm K2}(V) &= [1 + \exp(-83(V + 0.018 + V^{\tt shift}_{\rm K2}))]^{-1}. \end{aligned}$$

There are two principal parameters controlling the activity in the model of the individual burster: the magnitude of the external current $I_{\rm app}$ that affects the fast voltage dynamics, and the parameter $V^{\tt shift}_{\rm K2}$, which is the deviation from the experimentally averaged value, $V = -0.018\,{\rm V}$, corresponding to the half-activated gating channel for the slow potassium current. Both $I_{\rm app}$ and $V^{\tt shift}_{\rm K2}$ are independent bifurcation parameters. Their variations make the neuronal dynamics evolve and transition between tonic spiking, bursting and quiescence. In terms of dynamical system theory, these regimes are associated, respectively, with stable one- and two-time scale periodic orbits (that can become chaotic at bifurcations) and equilibrium states (respectively) in the phase space of the model. Figure 1 represents the $(V^{\tt shift}_{\rm K2}, I_{\rm app})$-biparametric sweep of the neuron model with use of the spike-counting method [26]. Its core is the quantification of spikes between consequent quiescent periods for given parameter values. The spike numbers are correspondingly color-coded in the bifurcation diagram (the bar on the right). This allows us to identify stability windows with fixed spike numbers, as well as to detect the borders on which spike numbers change. One can see these structures separated by spike-adding bifurcations [27,28] in fig. 1 with clearly demarcated regions corresponding to bursting, tonic-spiking and quiescence states. The sweep diagram is overlaid with several key curves that correspond to bifurcation transitions between different activity states [24]. These are the saddle-node, $SN_{\rm eq}$, bifurcation of equilibria between hyperpolarized quiescence and bursting; saddle-node limit cycles, $SN_{\rm lc}$, on the tonic-spiking and bursting boundary; the Andronov-Hopf,

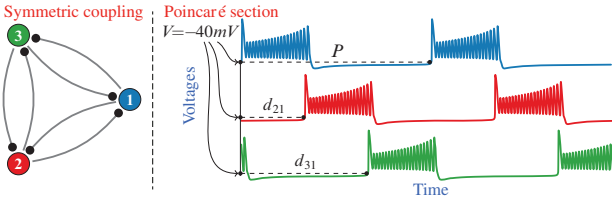

Fig. 2: (Color online) 3-cell network with symmetric synaptic connections generating voltage waveforms with clearly identified absolute phase lags $\{d_{21}, d_{31}\}$ relative to the reference burster 1.

$AH_{\rm eq}$, bifurcation on the boundary between depolarized quiescence and tonic spiking; and the homoclinic bifurcation, HB, giving rise to bistability of tonic spiking and bursting. The combined bifurcation diagram serves as a "road map" for individual ingredients (isolated neurons) to build a properly functioning model of a multifunctional CPG circuit [21].

The neurons in the 3-cell circuit are reciprocally coupled (via the term $I_{\rm syn}$) by non-delayed, fast chemical synapses described using the fast threshold modulation (FTM) paradigm as follows:

$$I_{\rm syn} = g^{\rm syn}(V_{\rm post} - E_{\rm syn})\Gamma(V_{\rm pre} - \Theta_{\rm syn}),$$
$$\Gamma(V_{\rm pre} - \Theta_{\rm syn}) = [1 + \exp(-1000(V_{\rm pre} - \Theta_{\rm syn}))]^{-1},$$

where $V_{\rm post}$ and $V_{\rm pre}$ are voltages of the post- and the presynaptic cells. Here, $g^{\rm syn} = -0.0004$ is a fixed coupling strength, $E_{\rm syn} = -0.0625\,{\rm V}$ and $\Theta_{\rm syn} = -0.03\,{\rm V}$ are the reversal potential and the synaptic threshold, respectively. We point out that alternative models of synapses, such as the α-synapse model, do not essentially alter the dynamical interactions between bursting cells [29].

"Fine" brute-force bifurcation analysis: location of burst jittering state. – Following [20,21], detailed studies of rhythms generated by neuronal circuits can be reduced, in the absence of noise, to the analysis of fixed points (FPs) and invariant circles (ICs) of Poincaré return maps for phase lags between constituent bursters. By choosing the first burster as the reference one, we introduce the absolute phase lags $\{d_{21}^{(n)}, d_{31}^{(n)}\}$, as shown by fig. 2. Once obtained the phase lags, we normalize them, $\varphi_{j1}^{(n)} = d_{j1}^{(n)}/P^{(n)}$, with $P^{(n)}$ the period or recurrent time) of the reference burster 1 on the n-bursting cycle, giving the relative phase lags $\{\varphi_{21}^{(n)}, \varphi_{31}^{(n)}\}$. Dense and even allocations of initial phase lags let us generate the desired 2D return map demonstrating time evolutions of phase lags transitioning toward stable FPs corresponding to phase-locked rhythms produced by the network under consideration.

In what follows, we will focus our consideration on the onset of a particularly remarkable rhythm that possesses not fixed, but periodically varying phase lags. Such a rhythm, called *phase jitter*, was frequently reported in coupled systems in nonlinear optics [30,31], as well as

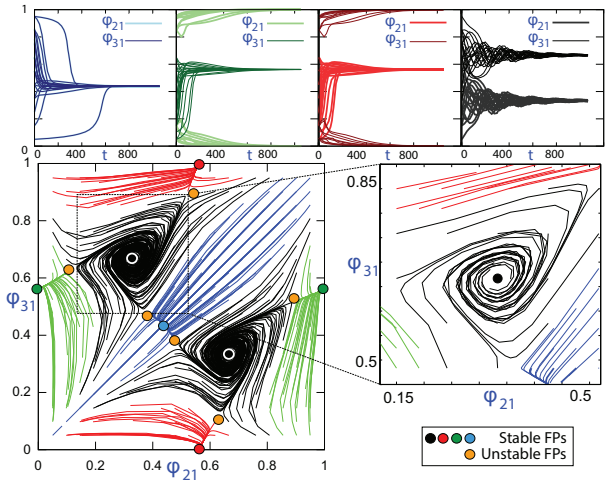

Fig. 3: (Color online) Progressions of phase lags of the network bursters converging to several fixed (locked) states (top panels), and the corresponding 2D map at $V_{\rm K2}^{\tt shift} = -0.01871$ with five stable FPs, and a magnification depicting a stable FP at $(\varphi_{21} = 1/3, \varphi_{31} = 2/3)$ with oscillatory convergence (bottom panels). Illustrative videos of the convergence of the 3-cell voltages V_i to all the different stable FP are shown as supplementary material: `Black-FP.mp4`, `Blue-FP.mp4`, `Green-FP.mp4` and `Red-FP.mp4`.

in neuroscience [21]. In the parameter space (fig. 1) of the bursters, these rhythms occur and persist on a short pathway $V_{\rm K2}^{\tt shift} \in [-0.01886, -0.01871]$ at the level $I_{\rm app} = 0.006$. The underlying bifurcations occurring in the 3-cell network are detailed in a series of 2D return map snapshots shown in figs. 3–5. Figure 3 depicts the progressions of representative phase lags converging to phase values (top panels), as well as the corresponding 2D map at $V_{\rm K2}^{\tt shift} = -0.01871$ (bottom panels). There are five stable FPs (color-coded dots and attraction basins) in this map. The coordinates of a stable FP correspond to a synchronized rhythm with phase lags locked at the specific values. The right-bottom panel is a magnification of the attraction basin of the FP corresponding to the clockwise (CW) traveling, or peristaltic rhythm, with phase lags locked at $(\varphi_{21} = 1/3, \varphi_{31} = 2/3)$. Respectively, the counterclockwise (CCW) traveling wave in the 3-cell network symmetrically corresponds to a stable FP at $(\varphi_{21} = 2/3, \varphi_{31} = 1/3)$ in the 2D map. Both FPs are stable foci with complex conjugate Floquet multipliers located within a unit circle, as evidenced by the spiral behavior of the trajectories nearby. The other three FPs are stable nodes to which transients converge more monotonically. Every such FP corresponds to the voltage waveform with locked phase lags where one interneuron bursts in anti-phase with the other two, which burst in-phase.

The critical value $V_{\rm K2}^{\tt shift} \simeq -0.018735$ corresponds to the occurrence of a secondary super-critical Andronov-Hopf (torus) bifurcation through which both CW and CCW FPs of the Poincaré map simultaneously become unstable. This bifurcation also gives rise to the emergence of

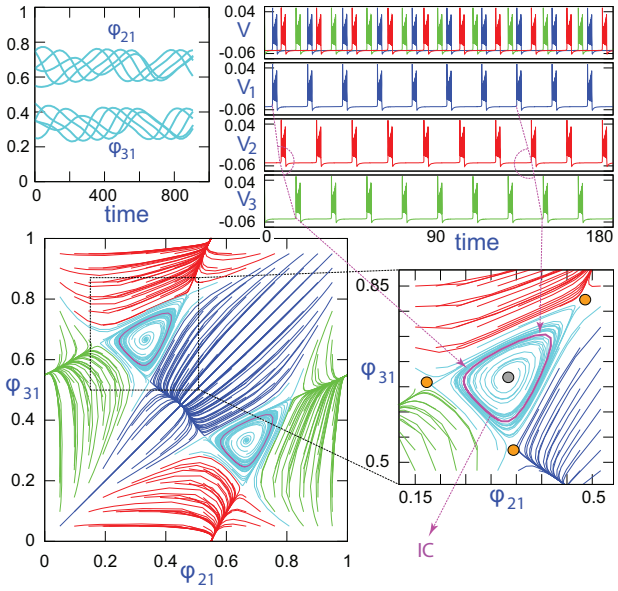

Fig. 4: (Color online) Progressions of phase lags of the network bursters exhibiting self-sustained oscillations associated with recurrent phase jitter in the voltage waveforms (top panels), and the corresponding 2D map at $V_{\mathrm{K2}}^{\mathtt{shift}} = -0.01876$, and a magnification depicting a stable IC around the unstable FP at ($\varphi_{21} = 1/3$, $\varphi_{31} = 2/3$) after the torus bifurcation (bottom panels). An illustrative video of the convergence of the 3-cell voltages V_i to the burst jittering state is shown as supplementary material: `Cyan-Jitter-IC.mp4`.

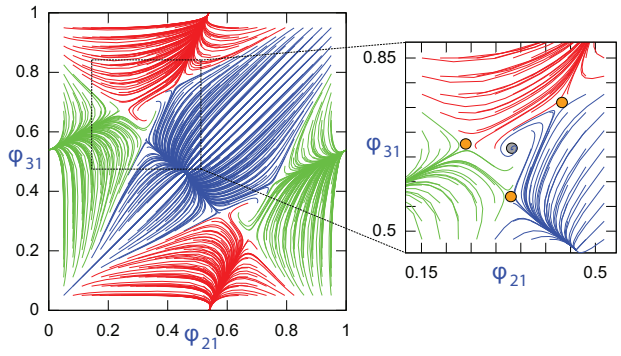

Fig. 5: (Color online) 2D Poincaré return map for phase lags at $V_{\mathrm{K2}}^{\mathtt{shift}} = -0.01886$, and its magnification near an unstable CW FP at ($\varphi_{21} = 1/3$, $\varphi_{31} = 2/3$) (after the heteroclinic bifurcation).

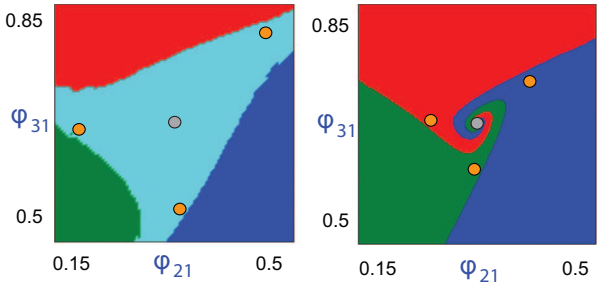

Fig. 6: (Color online) Attraction basins of the stable IC and FPs before, $V_{\mathrm{K2}}^{\mathtt{shift}} = -0.01876$ (left), and after, $V_{\mathrm{K2}}^{\mathtt{shift}} = -0.01886$ (right), the heteroclinic bifurcation, leading to dynamical uncertainty for nearby solutions.

a stable invariant curve (IC) bifurcating from each point. Each coexisting IC, which is made of either a finite number of periodic points or of infinitely many points, corresponds to quasi-periodic dynamics with two rationally or irrationally commensurable frequencies, respectively. The voltage waveforms, oscillations of phase lags and the corresponding map featuring a newly born pair of stable ICs are shown in fig. 4. One can see from the top panels that the depicted waveforms correspond to stable ICs that exhibit jitter with periodically varying phase lags.

As $V_{\mathrm{K2}}^{\mathtt{shift}}$ increases, the IC (and phase jitter, respectively) increases in size so that at -0.0187875 it becomes a closed heteroclinic connection between three saddle FPs nearby. The stable sets (separatrices) of these saddles bound the attraction basins of the remaining stable FPs (green, blue and red).

At the heteroclinic bifurcation, the outgoing separatrix of one saddle coalesces and then crosses over with the incoming separatrix of the other saddle. Due to the symmetry of the 3-cell network, there are two such heteroclinic connections in the 2D map. Each forms a closed heteroclinic cycle, similar to those occurring in $\mathbb{Z}_3$-symmetric systems [1]. Near this bifurcation, the number of iterates on each ICs increases while the phase points pass by the saddle FPs. As a result, this slows down the frequency of phase jitter near the corners of the heteroclinic cycle. The quasi-periodicity of bursting waveforms vanishes with the breakdown of heteroclinic cycles. This breakdown leads to a re-arrangement in the relative orientation between the stable and unstable separatrices of the saddle FPs. Before the bifurcation, the CW-FP (a stable focus) is an ω-limit set (as $n \to +\infty$) for unstable separatrices of the saddle FPs. After each heteroclinic cycle breaks down outwardly, an unstable focus FP becomes an α-limit set (as $n \to -\infty$) for stable separatrices of the near saddles. In other terms, the unstable separatrices that used to be oriented inward to spiral onto the stable CW-FP, become re-directed outward, tending to the remaining three stable FPs (see fig. 5). This gives rise to a peculiar phenomenon of dynamical uncertainty: an initial point taken near an unstable CW-FP will unpredictably spiral away converging to one of the stable FPs, as shown in fig. 6. For waveforms, this means that neither traveling rhythm is observable any longer, and that after a transition the network will begin stably generating one of the three antiphase bursting rhythms remaining in its repertoire.

The torus and heteroclinic cycle bifurcations in the 2D maps for phase lags determine the pivotal stages of the genesis of the bursting rhythms generated by a homogeneous circuit described by a 9D system of coupled ODEs. Other existing computational techniques would not allow one to predict and trace down the undergoing bifurcations

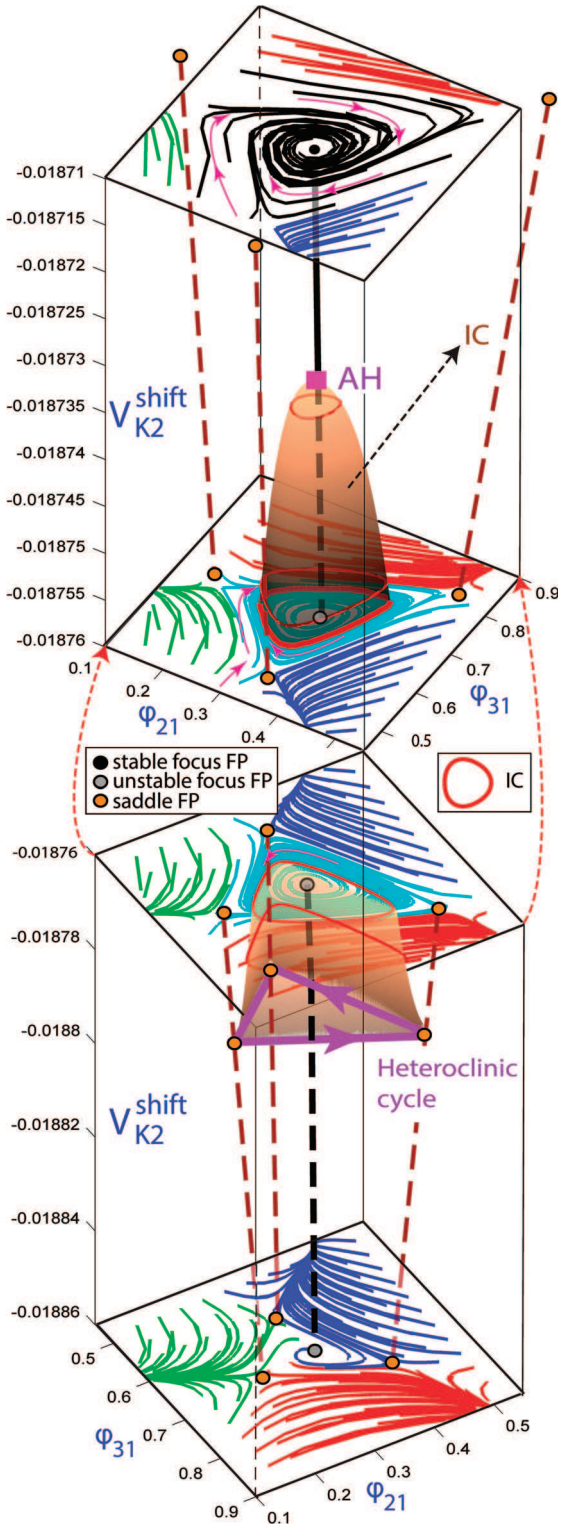

Fig. 7: (Color online) 3D bifurcation diagram revealing the torus and heteroclinic cycle bifurcations in the V_{K2}^{shift}-extended phase space of the 2D return maps for phase lags: a paraboloid-shaped surface being spanned by the stable ICs emerging through a supercritical torus (AH) bifurcation from the stable CW-FP. It is terminated by a heteroclinic cycle bifurcation. The parametric evolution of stable and unstable FPs is represented by solid and dashed lines (respectively).

in such a transparent and geometrically intuitive manner rather than using the Poincaré return maps for phase lags.

The use of parallel computational techniques available with utilization of multiple CPUs and/or Graphic Processor Units (GPUs) lets one reduce the necessary simulation time to merely seconds [32] for one plate of the progressions of phase lags of the network bursters. For instance, in our simulations we have selected a grid of 40×40 points in the $[0, 1) \times [0, 1)$ set. Each pair represents the initial conditions of the simulations, that is, the delays of the second and the third neuron with respect to one bursting of the first one. Computing these delays measured when crossing the Poincaré surface, we plot a line that represents the evolution of the bursting pattern. As the computation of each line is independent of the others, this task can be easily parallelized on any multi-core CPU and/or GPU device. In our plots we have computed 30 Poincaré sections for each neuron (a total of 90 points for each initial condition, and so a total of 144000 points per each 2D picture) with an error tolerance of 10^{-6} in the numerical ODE solver (the embedded Runge-Kutta method `DOPRI5(4)`), enough for this tough search. It is interesting to remark the great improvement on efficiency when computing using GPU devices (in our simulations around 85 times faster). In fact, the time reduction when GPU technology is used allows real-time simulations (note that a simulation time of 2 or 3 seconds per plot, as obtained in our case, is in such range of time).

Therefore, the use of parallel devices allows us to obtain in just a few minutes all the relevant data for studying a complete bifurcation analysis, where we have to compute a large number of such simulations changing one or several parameter values. This gives rise to new direct approaches to obtain bifurcation analysis. In our case, by extracting the relevant information from the big-data set (a set of 100 plates, each with 144000 points) to automatically detect the coordinates of both stable and unstable FPs as parameters of the network vary we have developed a new continuation technique. Having exhaustive information on FPs, ICs, heteroclinic cycles, attraction basins, etc., we have compiled a 3D bifurcation diagram representing the complete bifurcation route (fig. 7). This 3D diagram in the extended V_{K2}^{shift}-parameterized phase space is dissected in order to visualize the paraboloid-like surface spanned by the stable ICs emerging through a supercritical torus bifurcation from the stable CW-FP and terminating through the heteroclinic cycle bifurcation. The evolution of stable and saddle FPs is traced down by solid and dashed lines (respectively) representing the parametric dependence of their coordinates. This consolidated diagram (fig. 7) provides a wealth of information for in-depth understanding of the dynamics of the circuit constituted by three bursting neurons. The precise location of the bifurcation is obtained after a refinement process. That is, to accurately detect the bifurcation points we select the initial conditions of the network such that the first Poincaré events projected into the delay phase space are set close

to the (stable or unstable) point ($\varphi_{21} = 1/3$, $\varphi_{31} = 2/3$). By doing so, we can decide whether the phase trajectory converges to the stable targeted fixed point, or becomes repelled to converge to another attractor whether it is a point or an invariant cycle, associated with the burst jitter phenomenon.

Conclusions. – We have presented a case study of the onset and breakdown of phase jitter phenomena observed in bursting rhythms generated by a homogeneous 3-cell neuronal network. We have further developed a big-data computational approach for geometric interpretations disclosing all intrinsic structures, both dynamical and bifurcation ones, of the network under consideration. This approach permits us to discover detailed information exploiting the whole range of synchronized patterns. We have been able to predict and detect "stealth" bursting rhythms by tracing down invariant curves and heteroclinic cycles existing in the return map for phase lags. Both bifurcations provide the theoretical background necessary for understanding the universal phenomenon of phase jitter synchronization frequently reported in a range of diverse applications from physics and life sciences.

* * *

RB, MR and SS have been supported during this research by the Spanish Research projects MTM2012-31883 and MTM2015-64095-P, by the University of Zaragoza/CUD project UZCUD2015-CIE-05 and by the European Social Fund and Diputación General de Aragón (Grant E48). AS acknowledges the support from RFFI 11-01-00001, RSF grant 14-41-00044 at the Lobachevsky University of Nizhny Novgorod, and the grant in the agreement of August 27, 2013 N 02.B.49.21.0003 between The Ministry of Education and Science of the Russian Federation and Lobachevsky State University of Nizhni Novgorod (Sections 2-4), as well as NSF grant IOS-1455527. We thank J. Collens, A. Lozano, M. A. Martínez and K. Pusuluri for helpful discussions.

REFERENCES

[1] Ashwin P., Burylko O. and Maistrenko Y., *Physica D*, **237** (2008) 454.
[2] Aguiar M., Ashwin P., Dias A. and Field M., *J. Nonlinear Sci.*, **21** (2011) 271.
[3] Schwabedal J., Knapper D. and Shilnikov A., submitted to *Phys. Rev. E* (2015).
[4] Pais D., Caicedo-Núnez C. H. and Leonard N. E., *SIAM J. Appl. Dyn. Syst.*, **11** (2012) 1754.
[5] Zou W., Senthilkumar D. V., Zhan M. and Kurths J., *Phys. Rev. Lett.*, **111** (2013) 014101.
[6] Komarov M. and Pikovsky A., *Phys. Rev. Lett.*, **110** (2013) 134101.
[7] Hansel D., Mato G. and Meunier C., *Phys. Rev. E*, **48** (1993) 3470.
[8] Kori H. and Kuramoto Y., *Phys. Rev. E*, **63** (2001) 046214.
[9] Afraimovich V. S., Rabinovich M. I. and Varona P., *Int. J. Bifurcat. Chaos*, **14** (2004) 1195.
[10] Rabinovich M. I., Varona P., Tristan I. and Afraimovich V. S., *Front. Comput. Neurosci.*, **8** (2014).
[11] Selverston A., *Model Neural Networks and Behavior* (Springer, Berlin) 1985.
[12] Bal T., Nagy F. and Moulins M., *J. Comp. Physiol. A*, **163** (1996) 715.
[13] Marder E. and Calabrese R., *Physiol. Rev.*, **76** (1996) 687.
[14] Sakurai A., Gunaratne C. and Katz P., *J. Neurophysiol.*, **112** (2014) 1317.
[15] Alacam D. and Shilnikov A., *Int. J. Bifurcat. Chaos*, **25** (2015) 154003.
[16] Lewis T. and Rinzel J., *J. Comput. Neurosci.*, **14** (2003) 283.
[17] Gao J. and Holmes P., *J. Comput. Neurosci.*, **22** (2007) 39.
[18] Duan L., Fan D. and Lu Q., *Cogn. Neurodyn.*, **7** (2013) 341.
[19] Komarov M., Osipov G. and Zhou C., *Phys. Rev. E*, **87** (2013) 022909.
[20] Wojcik J., Clewley R. and Shilnikov A., *Phys. Rev. E*, **83** (2011) 056209.
[21] Wojcik J., Schwabedal J., Clewley R. and Shilnikov A. L., *PLoS ONE*, **9** (2014) e92918.
[22] Schwabedal J. T. C., Neiman A. B. and Shilnikov A. L., *Phys. Rev. E*, **90** (2014) 022715.
[23] Jalil S., Allen D., Youker J. and Shilnikov A., *Chaos*, **23** (2013) 046105.
[24] Shilnikov A., *Nonlinear Dyn.*, **68** (2012) 305.
[25] Hodgkin A. L. and Huxley A. F., *J. Physiol.*, **117** (1952) 500.
[26] Barrio R. and Shilnikov A., *J. Math. Neurosci.*, **1** (2011) 6.
[27] Barrio R., Martínez M. A., Serrano S. and Shilnikov A., *Chaos*, **24** (2014) 023128.
[28] Barrio R., Lefranc M., Martínez M. A. and Serrano S., *EPL*, **109** (2015) 20002.
[29] Jalil S., Belykh I. and Shilnikov A., *Phys. Rev. E*, **85** (2012) 036214.
[30] Brabec T. and Krausz F., *Rev. Mod. Phys.*, **72** (2000) 545.
[31] Goulielmakis E., Schultze M., Hofstetter M., Yakovlev V. S., Gagnon J., Uiberacker M., Aquila A. L., Gullikson E. M., Attwood D. T., Kienberger R., Krausz F. and Kleineberg U., *Science*, **320** (2008) 1614.
[32] Rodríguez M., Blesa F. and Barrio R., *Comput. Phys. Commun.*, **192** (2015) 228.